JACS
JOURNAL OF THE AMERICAN CHEMICAL SOCIETY
Communication
pubs.acs.org/JACS

Selective Growth of Subnanometer Diameter Single-Walled Carbon Nanotube Arrays in Hydrogen-Free CVD

Lixing Kang,[†,‡,§] Shibin Deng,[†] Shuchen Zhang,[†] Qingwen Li,[‡] and Jin Zhang*[,†]

[†]Center for Nanochemistry, Beijing Science and Engineering Center for Nanocarbons, Beijing National Laboratory for Molecular Sciences, College of Chemistry and Molecular Engineering, Peking University, Beijing 100871, P. R. China

[‡]Division of Advanced Nanomaterials, Suzhou Institute of Nanotech and Nanobionics, Chinese Academy of Sciences, Suzhou 215123, P. R. China

[§]University of Chinese Academy of Sciences, Beijing 100049, P. R. China

Supporting Information

ABSTRACT: Small diameter single-walled carbon nanotube (SWNT) arrays with larger bandgap are more desirable as near-infrared optical absorbers for the fabrication of high performance photovoltaic and photodetector devices. We report herein a rational approach to selective growth of well-aligned subnanometer diameter (~84% between 0.75 and 0.95 nm) SWNT arrays with a density of 0.3−0.5 tubes/μm on quartz surfaces using solid Mo_2C catalysts for short-time growth by low carbon feeding in hydrogen-free CVD. These subnanometer diameter SWNTs have a narrow chirality distribution (the ratio of (8,4), (8,5) and (7,6) is higher than 73%). During nanotube growth, only small size Mo nanoparticles are carbonized into stable Mo_2C for catalyzing the growth of SWNTs through low carbon feeding rate over short time in the hydrogen-free environment, whereas larger catalysts are inactive due to underfeeding. Meanwhile, solid Mo_2C catalysts are effective in reducing the chirality distributions of the as-grown SWNTs. Additionally, combining an annealing process after loading catalyst on the sapphire substrates, the average density is increased to ~15 tubes/μm while maintaining small diameter and narrow chirality distribution. Our results offer more choices for structurally controlled growth of aligned-SWNTs, with potential applications in nanoelectronics.

The main hurdle in the application of single-walled carbon nanotube (SWNT) based nanoelectronics is the lack of control over their structure, more precisely their diameter and eventually chirality.[1] Diameter control is fundamental yet indispensable, because the tube diameter is closely related to the energy band structure. For a semiconducting SWNT (s-SWNT), the bandgap is inversely proportional to the tube diameter.[2] Small diameter (we refer to ≤1 nm in this paper) s-SWNTs have relatively large bandgaps (~1.0 eV), which give them exceptionally high on/off ratio and fast spectral response, pointing to promising applications in various specific nanoelectronic applications, such as photovoltaic and photodetector near-infrared-based devices.[3] Furthermore, the small diameter control is an essential step toward chirality control, which often accompany narrow chirality distribution using suitable catalysts.[4]

In a chemical vapor deposition (CVD) system, catalysts and experimental parameters (including temperature, gas composition and flow rate) are the most important factors influencing the diameters of the SWNTs.[1] According to the widely accepted view, the size of the catalysts directly define the diameter of nanotubes.[5] During the high temperature nanotube growth process, traditional metal nanoparticle catalysts always undergo thermal coalescence or Ostwald ripening,[6,7] especially on flat substrates, which generally result in an increase of the SWNT diameter (typical results exceed 1 nm) and broadening of their size distribution. On the other hand, high melting point solid catalysts such as tungsten and molybdenum based compounds can maintain their crystalline structure during the CVD process. They have been shown to be effective in reducing the diameter and chirality distributions, even obtaining high percentage specific chirality.[8,9] Unfortunately, it is still very hard to obtain uniform solid catalysts with subnanometer size. Recently, epitaxial growth from well-defined seeds, such as short nanotubes[10] and carbon nanorings,[11] has been found to control the diameter of SWNTs precisely. However, these routes suffer shortcomings of either low yield or poor alignment of nanotubes.

Hydrogen is another vital role during the SWNT nucleation stage in the CVD process. It has been proposed that H_2 can lower the carbon deposition on the catalyst surface through hydrogenation reaction to affect sp^2 C formation.[12] Losing the protection of sufficient carbon deposition, the small nanoparticles were unstable and aggregated with each other, leading to the formation of the nanotube cap occurring at a larger diameter catalyst. Therefore, a hydrogen-free environment in the SWNT nucleation and growth process, we call "hydrogen-free CVD", will be beneficial to the synthesis of small diameter SWNT arrays. In addition, a low carbon feeding rate over a short time will allow only small particles to obtain enough carbon to nucleate SWNTs, whereas larger particles are underfed and inactive.[13] To magnify further differences of nucleation rate between small and large diameter catalysts and reduce the chirality distributions, Mo nanoparticles, which can be gradually carbonized into stable Mo_2C in a carbon atmosphere,[9] should be chosen as catalysts. Following this

Received: June 22, 2016
Published: September 21, 2016

DOI: 10.1021/jacs.6b06477
J. Am. Chem. Soc. 2016, 138, 12723−12726

thinking, we demonstrate that it is possible to obtain small diameter SWNT arrays with narrow chirality distribution by using solid Mo_2C as catalysts for short time growth by low carbon feeding in hydrogen-free CVD.

Figure 1a schematically shows the growth procedure of this approach. Polydisperse Mo nanoparticles were gradually

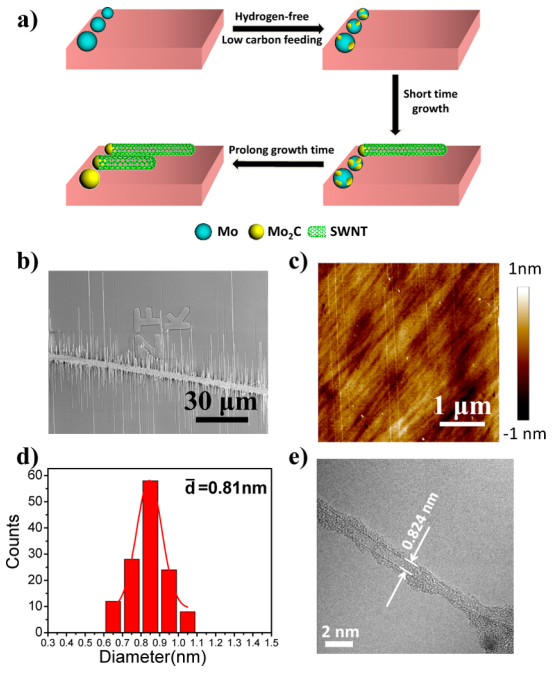

Figure 1. (a) Schematic illustration of selective growth of small diameter SWNTs. (b) Typical SEM image of the as-grown SWNT array. (c) AFM analysis of SWNTs on the quartz substrate. The diameters of different nanotubes are almost identical and do not exceed 1 nm. (d) Corresponding diameter distribution of the SWNTs. (e) TEM image of an individual SWNT from the as-grown sample.

carbonized by feeding a low carbon source in the hydrogen-free environment. In a short time, small diameter Mo nanoparticles were first fully carbided into Mo_2C and then catalyzed the growth of small diameter SWNTs. With further extension of the growth time, the large diameter Mo nanoparticles also changed into Mo_2C and large diameter SWNTs appeared. Thus, we can selectively grow small diameter SWNTs by low carbon feeding in a short time without hydrogen during the growth process. Figure 1b shows a typical scanning electron microscopy (SEM) image of the as-grown well-aligned SWNTs with average density 0.3−0.5 tubes/μm under the optimal growth condition (20 sccm Ar through an ethanol bubbler for growth of 2 min, for more details of the CVD process see the Experimental Section). Atomic force microscopy (AFM) measurements (Figure 1c,d) indicated the overwhelming majority of nanotube diameters were less than 1 nm and with a narrow distribution 0.81 ± 0.2 nm. Over 80% of the nanotube diameters were between 0.75 and 0.95 nm though the diameters of catalysts were in a wide range from 0.4 to 3 nm (Figure S1). In order to measure the nanotube diameter more accurately, the SWNT arrays grown on a quartz surface were transferred onto a copper grid for high-resolution transmission electron microscopy (HRTEM) characterization. Figure 1e is a representative TEM image of an individual nanotube (for more TEM images, see Figure S2a). Statistics of TEM measurements (Figure S2b) showed most nanotube diameters were concentrated at 0.84 ± 0.2 nm, consistent with the results obtained by AFM.

To obtain further structural information on the nanotubes, the SWNT arrays grown on quartz were transferred onto SiO_2/Si substrates with 90 nm SiO_2 for Raman measurement. In Figure 2a,b, typical radial breathing mode (RBM) peaks of the

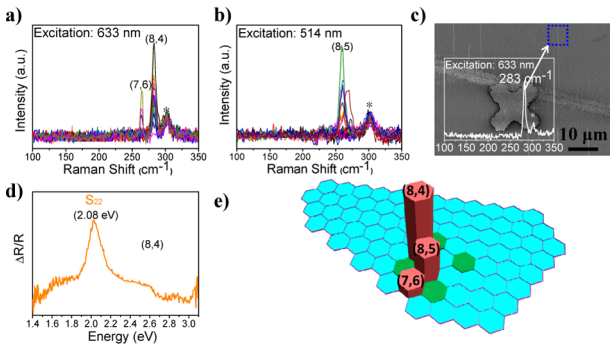

Figure 2. (a,b) Raman spectra in the RBM region of the nanotubes measured with 633 and 514 nm lasers. The peaks denoted by black asterisks are from the SiO_2/Si substrate. (c) SEM image of the transferred SWNT arrays on SiO_2/Si Substrates. The inset shows the Raman spectra of an individual SWNT in the blue dashed box. (d) Corresponding reflection optical spectrum of the same nanotubes with the help of marks on the SiO_2/Si substrate. (e) Chiral map for the SWNTs grown for short time in a hydrogen-free environment.

Raman spectra with different wavelength excitations showed three distinct peaks, 283 and 264 cm^{-1} with a 633 nm laser (Figure 2a), and 260 cm^{-1} with a 514 nm laser (Figure 2b). According to the relationship between the RBM frequency and SWNT diameter,[14] the diameter distributions were calculated to be 0.85 ± 0.1 nm, in the range of AFM and TEM measurements. In addition, the shoulder peaks of G$^-$ band shifting toward lower frequencies (<1540 cm^{-1}) further confirmed the subnanometer diameter of the nanotubes in arrays (Figure S3).[15] As for their chirality assignments by Raman spectra are comparatively reliable, because adjacent SWNTs in Kataura plot have very distinct transition energy values and RBM frequencies for such small diameter SWNTs.[16] Taking a RBM peak deviation of ±2 cm^{-1}, only three possible chiralities (8,4), (7,6) and (8,5) are located in the corresponding region by comparing with Kataura plot.[16] These chirality assignments were further verified by the newly developed optical reflection spectrum measurement of individual SWNTs.[17,18] Figure 2c shows an isolated SWNT on the substrate with a RBM peak at 283 cm^{-1}. From the corresponding reflection optical spectrum (Figure 2d), the transition energies at the optical resonance peaks were identified as 2.08 eV, corresponding to the second van Hove singularity transition (S_{22}) of a (8,4) nanotube according to the atlas of carbon nanotube optical transitions (for details, see the Experimental Section).[17] Other chirality assignments ((7,6) and (8,5)) by optical reflection spectrum are shown in Figure S4.

To estimate the chirality distribution, we used SEM to confirm the location of SWNTs on the marked substrate from multibatch samples and counted all 348 nanotubes. Then Raman line mapping (1 μm laser spot at a step of 1 μm) with different lasers (514, 633 and 785 nm) at the same place were performed to detect 302 resonant RBM signals (Table S1 in Supporting Information). Statistics on the times of observed

DOI: 10.1021/jacs.6b06477
J. Am. Chem. Soc. 2016, 138, 12723−12726

different RBM peaks and the corresponding (n,m) for the SWNT samples are shown in Table S2. The major chiralities of (8,4), (8,5) and (7,6) accounted for 46.6%, 17.5% and 8.9%, respectively. The calculation of chirality content was based on the total number of SWNTs in the SEM images. The chirality distribution of the as-grown SWNT samples was more visually apparent in the chiral map (Figure 2e). These results demonstrated small diameter SWNT arrays with narrow-chirality distribution were successfully obtained by low carbon feeding for short time growth in hydrogen-free CVD.

To understand better the hypothesis of selective nucleation for the growth of small diameter SWNTs with narrow-chirality distribution, we performed certain control experiments. First, we prolonged the growth time to 5 min. The average density of the SWNT arrays obviously improved, up to 2−3 tubes/μm as shown in the SEM image of Figure 3a. At the same time, we

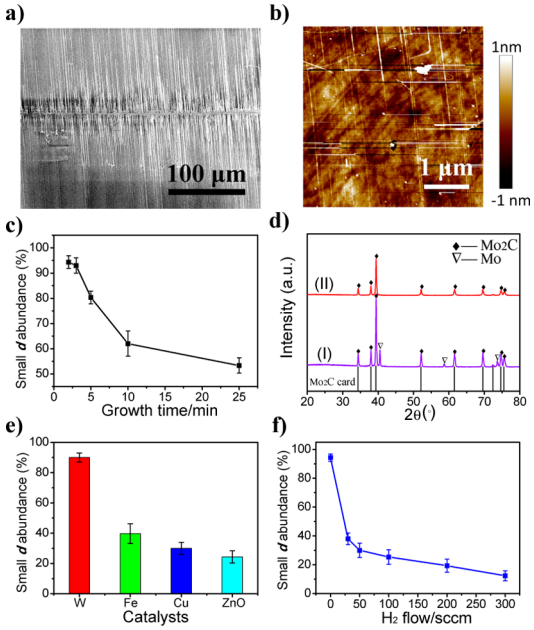

Figure 3. (a) SEM image of SWNTs obtained by prolonging the growth time. (b) AFM image of SWNT arrays near the catalyst stripe. Some nanotubes with diameter larger than 1 nm appear. (c) Statistics of small diameter (≤1 nm) SWNT abundance in the as-grown SWNT arrays at different growth time. (d) XRD patterns of catalysts after hydrogen reduction and reaction with ethanol for different times (curve I, 2 min; curve II, 5 min). The black curve presents the standard card of Mo_2C. (e,f) Selectivity of small diameter SWNTs using different catalysts and at different hydrogen flow.

detected many >1 nm diameter SWNTs by AFM and Raman (Figure 3b and Figure S5). Further increasing the growth time continued to reduce the abundance of small diameter SWNTs (Figure 3c). These results indicated the small diameter catalysts were nucleating faster than large diameter catalysts. According to the reported literature and our previous study,[9,19] calcined Mo species catalysts supported on a substrate were reduced to Mo by hydrogen at elevated temperature followed by carbonization into Mo_2C on introduction of a carbon source. During the carbonization process, the carbon species first adsorbed on the surface of Mo nanoparticles and gradually diffused into the bulk to form Mo_2C. This process was confirmed by the XRD patterns (Figure 3d). The formation of Mo_2C was further confirmed by HRTEM (Figure S6). Because of the strong C−Mo bond, the surface carbon was hard to desorb from Mo nanoparticles, especially in the hydrogen-free environment. Thus, only the Mo was fully carbided into Mo_2C, after which excess carbon could form the cap of a nanotube and initiate the growth of SWNT. The time of full carbonization decreases as the size of Mo nanoparticles decreases. Therefore, a high percent of small diameter Mo nanoparticles preferentially nucleated and catalyzed the growth of SWNTs in a short time by low carbon feeding.

We also used other catalysts, such as W, Fe, Cu and ZnO for short time growth in the hydrogen-free environment. Typical SEM images of SWNT arrays from different catalysts are shown in Figure S7. The enrichment of small diameter SWNTs can also be achieved from W catalysts (Figure 3e). The binding strength of C to Mo and W is strong and both catalysts can form stable solid carbides during the growth of SWNTs.[19] However, the interactions between C and other catalysts (Fe, Cu and ZnO) are weaker than Mo or W catalysts,[19] indicating that differences of nanotube nucleation rate between different size catalysts become reduced. As a consequence, these catalysts resulted in a considerable decrease in the abundance of small diameter SWNTs (Figure 3e). A similar trend was observed when increasing the flow rate of Ar through an ethanol bubbler (Figure S8). In addition, the content of small diameter SWNTs declined sharply when introducing hydrogen in the growth process (Figure 3f and Figure S9). The presence of hydrogen abated the interactions between C and catalysts and allowed carbon species to desorb more easily from catalysts.[20] This leaded the small catalysts to aggregate and grow large diameter SWNTs. To distinguish the roles of hydrogen and the hydrogen component in ethanol for the selective growth of small diameter SWNTs, a carbon source without hydrogen such as carbon monoxide was substituted for ethanol. Although the density of SWNT arrays decreased using CO as the carbon feeding gas in comparison to ethanol (Figure S10a), the percentage of small diameter SWNTs in the arrays was above 91% according to the statistics by AFM and multiwavelength laser (Figure S10b,d). Especially, some other SWNTs with smaller diameter appeared and could be detected by Raman spectrometer (Figure S10c). These results demonstrated the hydrogen indeed inhibited small diameter SWNT growth.

The selective nucleation method provides a new strategy for SWNT control growth. Recently, our group found the density of SWNTs increased obviously through an annealing process after loading the catalyst on the sapphire substrate.[21] We combined these two methods in this study to obtain dense small diameter SWNT arrays (details of the growth process are described in the Experimental Section). From SEM observations (Figure 4a), uniform and perfectly aligned SWNT arrays covered the sapphire surface with an average density around 15 tubes/μm. AFM image of the as-grown SWNTs (Figure 4b) and the corresponding diameter distribution (Figure 4c) showed the diameters of most SWNTs were less 1 nm and with a narrow distribution 0.85 ± 0.2 nm. Raman measurements with multiple excitation lasers (Figure 4d and Figure S11a) further indicated the main chairities were (8,4), (7,6) and (8,5), which were consistent with the growth result on quartz. Furthermore, extension of the growth time also resulted in lower abundance of small diameter SWNTs (Figure S11b,c).

The essence of the selective nucleation method is to optimize CVD conditions and maximize the differences of nucleation rate between different sizes of catalysts, which is not limited to any kind of carbon nanotube growth. It could also be applicable

DOI: 10.1021/jacs.6b06477
J. Am. Chem. Soc. 2016, 138, 12723−12726

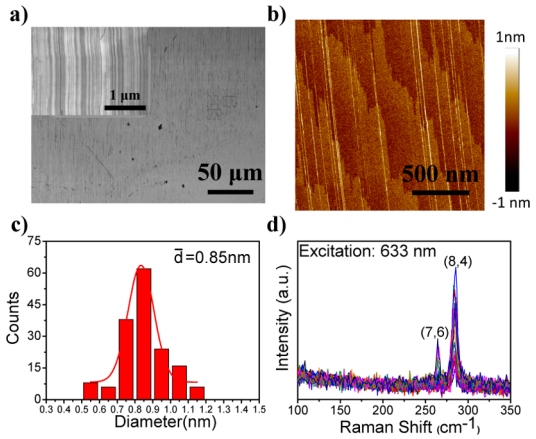

Figure 4. (a) SEM image of SWNT array on sapphire by short time growth in a hydrogen-free environment. (b) AFM image of dense small diameter SWNT arrays on the sapphire substrate. (c) Diameter distribution of the as-grown SWNTs. (d) RBM peaks of Raman spectra for the SWNT samples measured directly on the sapphire substrate with a 633 nm laser.

to the catalyst-assisted control synthesis of other nanomaterials, such as boron nitride nanotubes, silicon nanowires, zinc oxide nanorods and so on.

In summary, a straightforward and effective method was developed to obtain directly small diameter (0.81 ± 0.2 nm) SWNT arrays with narrow chirality distribution ((8,4), (8,5) and (7,6) were the major chiralities) on a single crystal substrate. Detailed experiments and analysis reveal that small diameter Mo catalyst selective nucleation can be realized by low carbon feeding rate in hydrogen-free CVD for short time growth. Additionally, this strategy can be applied on sapphire for the selective growth of dense small diameter SWNT arrays with narrow chirality distribution. These results offer more valuable insight into the selective growth mechanism of SWNTs and could be taken as a universal method for structure-control synthesis of other one-dimensional nanomaterials.

■ ASSOCIATED CONTENT

Supporting Information

The Supporting Information is available free of charge on the ACS Publications website at DOI: 10.1021/jacs.6b06477.

Experimental details, characterization methods, supplementary figures (PDF)

■ AUTHOR INFORMATION

Corresponding Author

*jinzhang@pku.edu.cn

Notes

The authors declare no competing financial interest.

■ ACKNOWLEDGMENTS

This work was financially supported by the National Natural Science Foundation of China (grant 51432002, 21129001, 21233001) and the Ministry of Science and Technology of China (2016YFA0200101 and 2016YFA0300903).

■ REFERENCES

(1) Chen, Y. B.; Zhang, Y. Y.; Hu, Y.; Kang, L. X.; Zhang, S. C.; Xie, H. H.; Liu, D.; Zhao, Q. C.; Li, Q. W.; Zhang, J. *Adv. Mater.* **2014**, *26*, 5898.

(2) Saito, R.; Dresselhaus, G.; Dresselhaus, M. S. *Phys. Rev. B: Condens. Matter Mater. Phys.* **2000**, *61*, 2981.

(3) Bindl, D. J.; Wu, M. Y.; Prehn, F. C.; Arnold, M. S. *Nano Lett.* **2011**, *11*, 455.

(4) Bachilo, S. M.; Balzano, L.; Herrera, J. E.; Pompeo, F.; Resasco, D. E.; Weisman, R. B. *J. Am. Chem. Soc.* **2003**, *125*, 11186.

(5) Li, Y. M.; Kim, W.; Zhang, Y. G.; Rolandi, M.; Wang, D. W.; Dai, H. J. *J. Phys. Chem. B* **2001**, *105*, 11424.

(6) Amama, P. B.; Pint, C. L.; McJilton, L.; Kim, S. M.; Stach, E. A.; Murray, P. T.; Hauge, R. H.; Maruyama, B. *Nano Lett.* **2009**, *9*, 44.

(7) Pisana, S.; Cantoro, M.; Parvez, A.; Hofmann, S.; Ferrari, A. C.; Robertson, J. *Phys. E* **2007**, *37*, 1.

(8) Yang, F.; Wang, X.; Zhang, D. Q.; Yang, J.; Xu, Z. W.; Wei, J. K.; Wang, J.-Q.; Xu, Z.; Peng, F.; Li, X. M.; Li, R. M.; Li, Y. L.; Li, M. H.; Bai, X. D.; Ding, F.; Li, Y. *Nature* **2014**, *510*, 522.

(9) Zhang, S.; Tong, L.; Hu, Y.; Kang, L.; Zhang, J. *J. Am. Chem. Soc.* **2015**, *137*, 8904.

(10) Yao, Y. G.; Feng, C. Q.; Zhang, J.; Liu, Z. F. *Nano Lett.* **2009**, *9*, 1673.

(11) Omachi, H.; Nakayama, T.; Takahashi, E.; Segawa, Y.; Itami, K. *Nat. Chem.* **2013**, *5*, 572.

(12) Zhang, G. Y.; Mann, D.; Zhang, L.; Javey, A.; Li, Y. M.; Yenilmez, E.; Wang, Q.; McVittie, J. P.; Nishi, Y.; Gibbons, J.; Dai, H. J. *Proc. Natl. Acad. Sci. U. S. A.* **2005**, *102*, 16141.

(13) Lu, C.; Liu, J. *J. Phys. Chem. B* **2006**, *110*, 20254.

(14) Liu, B.; Liu, J.; Li, H.-B.; Bhola, R.; Jackson, E. A.; Scott, L. T.; Page, A.; Irle, S.; Morokuma, K.; Zhou, C. *Nano Lett.* **2015**, *15*, 586.

(15) Telg, H.; Duque, J. G.; Staiger, M.; Tu, X.; Hennrich, F.; Kappes, M. M.; Zheng, M.; Maultzsch, J.; Thomsen, C.; Doorn, S. K. *ACS Nano* **2012**, *6*, 904.

(16) Dresselhaus, M. S.; Dresselhaus, G.; Saito, R.; Jorio, A. *Phys. Rep.* **2005**, *409*, 47.

(17) Liu, K.; Deslippe, J.; Xiao, F.; Capaz, R. B.; Hong, X.; Aloni, S.; Zettl, A.; Wang, W.; Bai, X.; Louie, S. G.; Wang, E.; Wang, F. *Nat. Nanotechnol.* **2012**, *7*, 325.

(18) Deng, S.; Tang, J.; Kang, L.; Hu, Y.; Yao, F.; Zhao, Q.; Zhang, S.; Liu, K.; Zhang, J. *Adv. Mater.* **2016**, *28*, 2018.

(19) Ding, F.; Larsson, P.; Larsson, J. A.; Ahuja, R.; Duan, H.; Rosén, A.; Bolton, K. *Nano Lett.* **2008**, *8*, 463.

(20) Lolli, G.; Zhang, L.; Balzano, L.; Sakulchaicharoen, N.; Tan, Y.; Resasco, D. E. *J. Phys. Chem. B* **2006**, *110*, 2108.

(21) Hu, Y.; Kang, L. X.; Zhao, Q. C.; Zhong, H.; Zhang, S. C.; Yang, L. W.; Wang, Z. Q.; Lin, J. J.; Li, Q. W.; Zhang, Z. Y.; Peng, L. M.; Liu, Z. F.; Zhang, J. *Nat. Commun.* **2015**, *6*, 6099.

DOI: 10.1021/jacs.6b06477
J. Am. Chem. Soc. 2016, 138, 12723−12726